

*Series Editor*  
*Robert Baptist*

---

# **Neuro-inspired Information Processing**

---

Alain Cappy

Color section

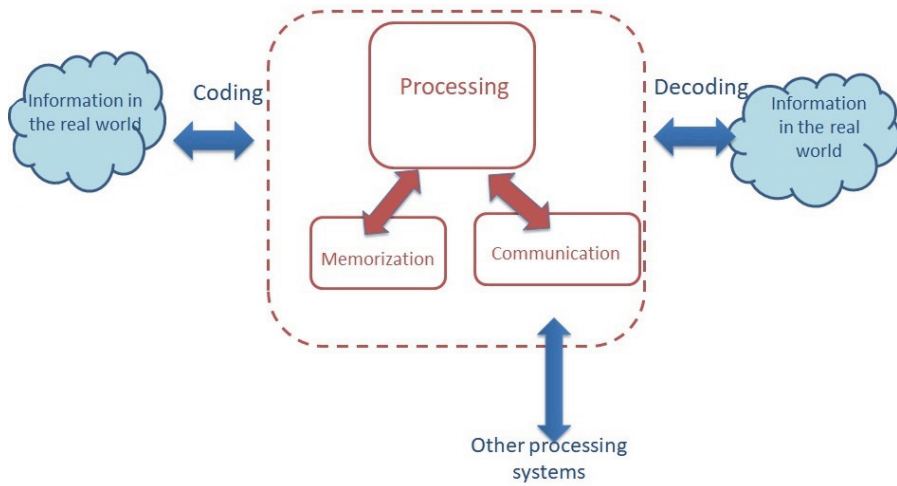


**Figure 1.1.** *Block diagram of information processing systems*

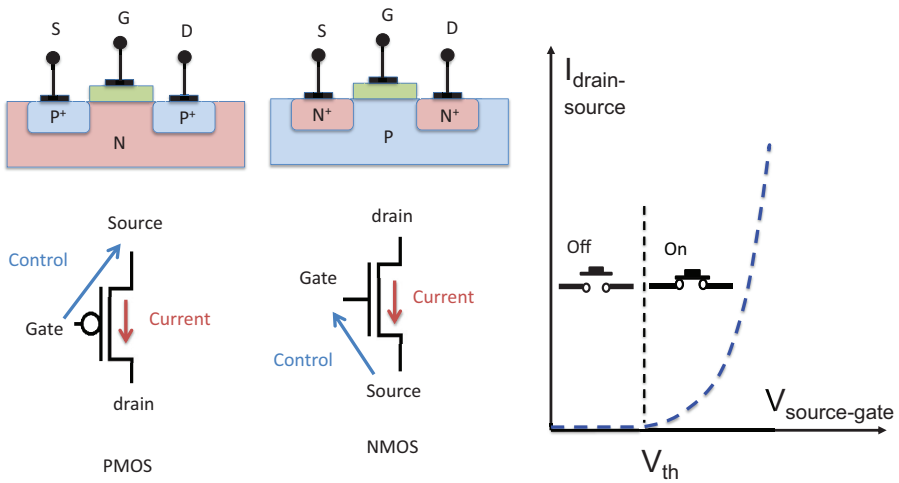


**Figure 1.5.** Physical and electrical diagrams of NMOS and PMOS transistors. Current–voltage characteristic of a MOS transistor.  $V_{\text{th}}$  is the threshold voltage

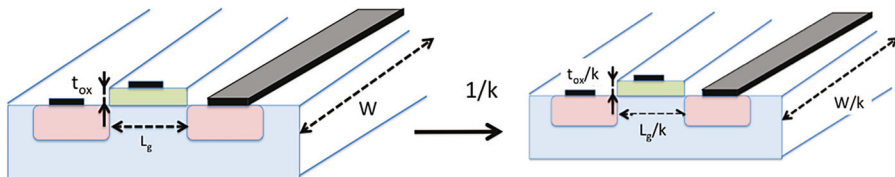


**Figure 1.7.** Principle of downscaling. All dimensions and voltages are divided by the same factor,  $k$ , while the semiconductor doping is multiplied by  $k$

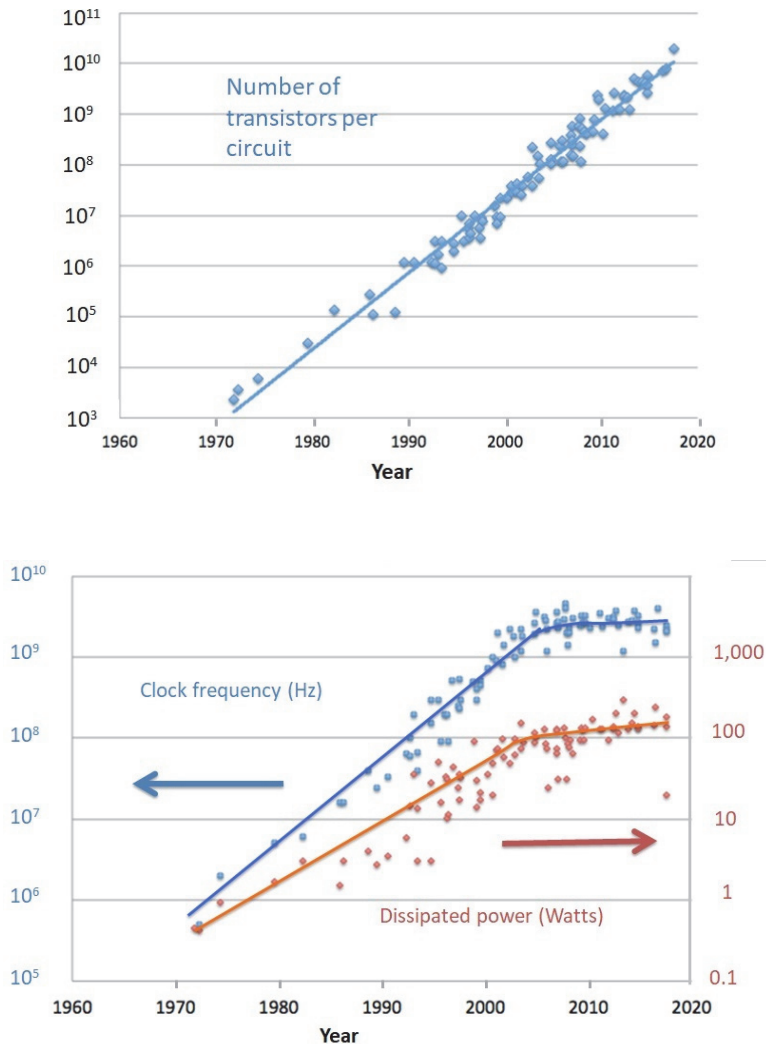


**Figure 1.8.** Evolution in the number of transistors, clock frequency and total power dissipated by a microprocessor over 50 years. Each point corresponds to a specific microprocessor. The data up to 2010 were collected by H. Horowitz, F. Labonte, O. Shacham, K. Olukotun, L. Hamond and C. Batten and the data for 2010–2017 by K. Rupp. Source: <https://www.karlsruhp.net/2018/02/42-years-of-microprocessor-trend-data/>



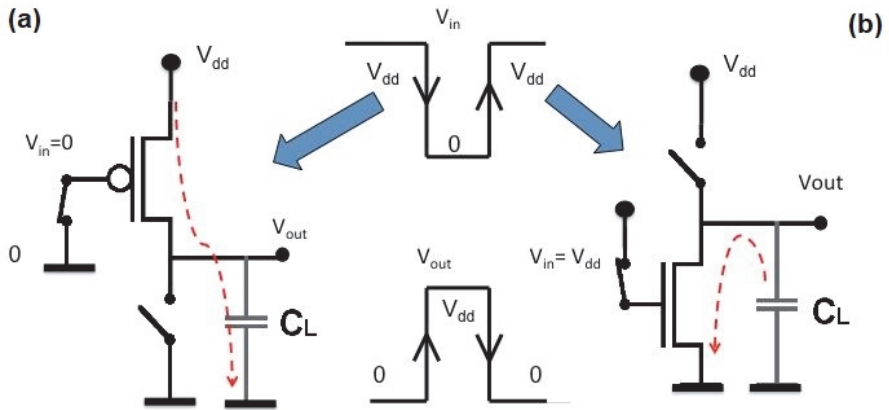


**Figure 1.9.** Switching of a CMOS inverter. Charge and discharge currents of the capacitance,  $C_L$

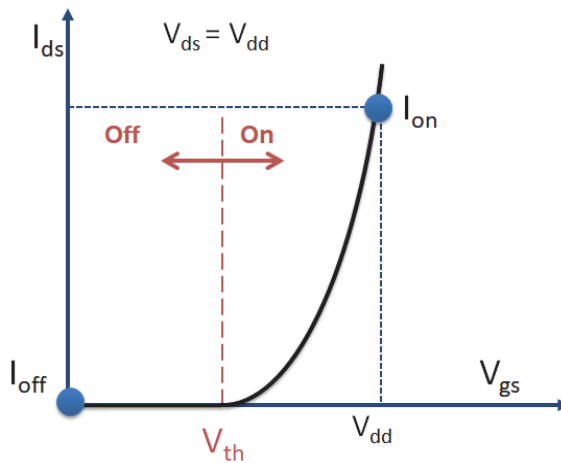


**Figure 1.10.** Drain-source current of an NMOS as a function of the control voltage,  $V_{gs}$ . The drain-source voltage is  $V_{dd}$ . In a simple model of the transistor,  $I_{ds} = K \cdot (V_{gs} - V_{th})^2$  beyond the threshold ( $V_{gs} > V_{th}$ ). A similar curve is obtained for a PMOS by replacing  $I_{ds}$ ,  $V_{ds}$  and  $V_{gs}$  with  $I_{sd}$ ,  $V_{sg}$  and  $V_{sd}$

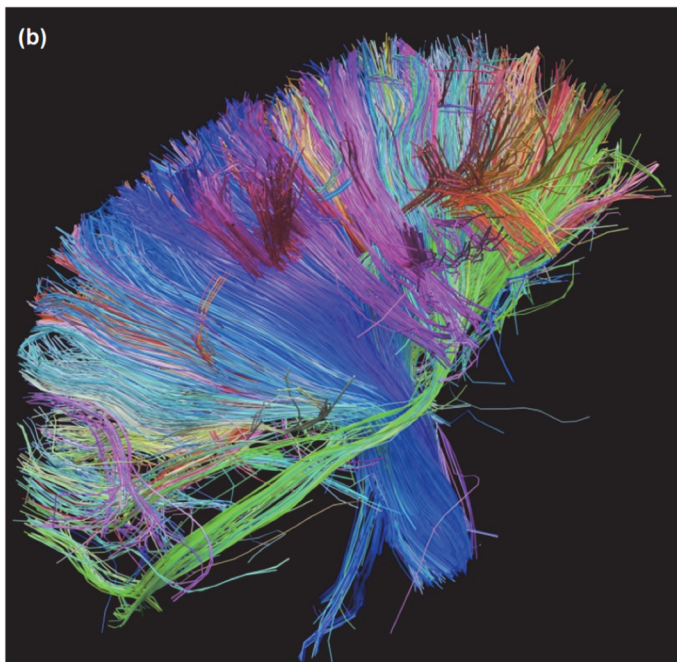
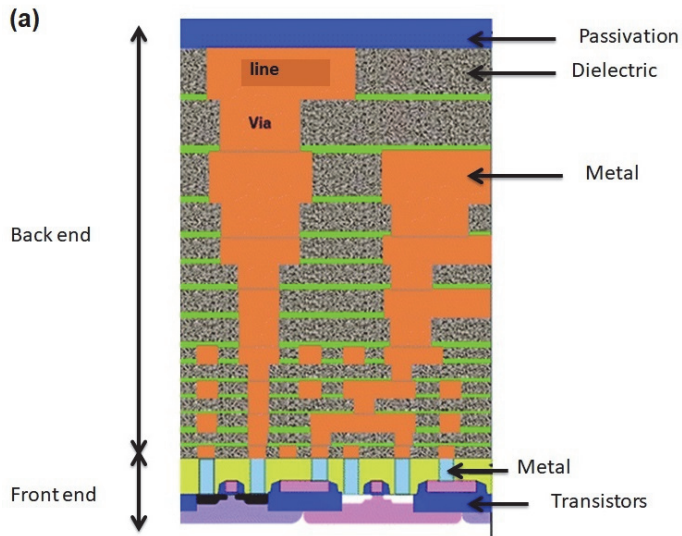


**Figure 1.16.** (a) Diagram of interconnections within an integrated circuit; (b) architecture of connections in the white matter of the brain. The colors specify the direction: red = left/right, green = forward/back, blue = up/down. (Source: [www.humanconnectomeproject.org](http://www.humanconnectomeproject.org))

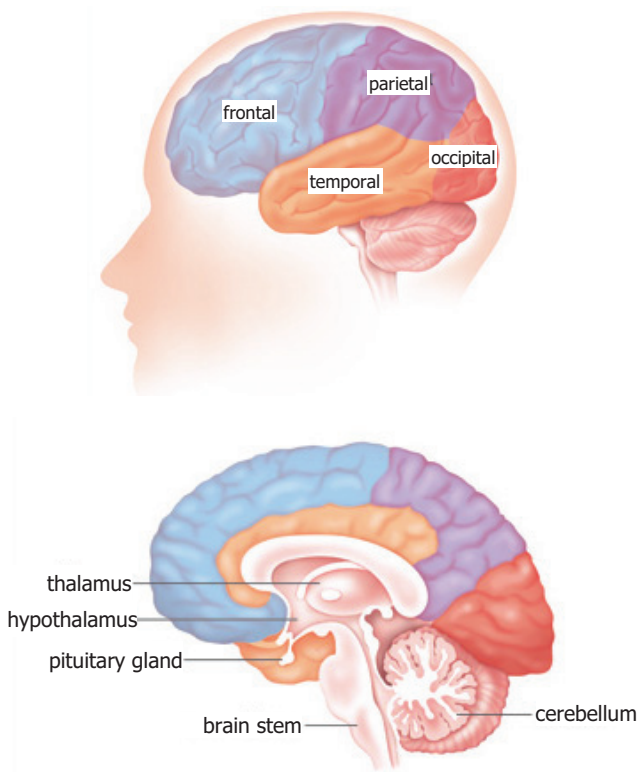


**Figure 2.1.** *The lobes of the left hemisphere and cross-sectional view of the brain*

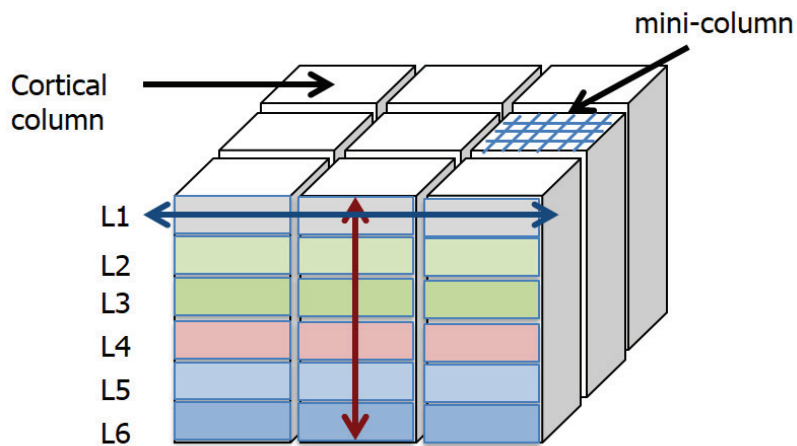


**Figure 2.3.** Detail of cortical layers, L1–L6. Columns and mini-columns

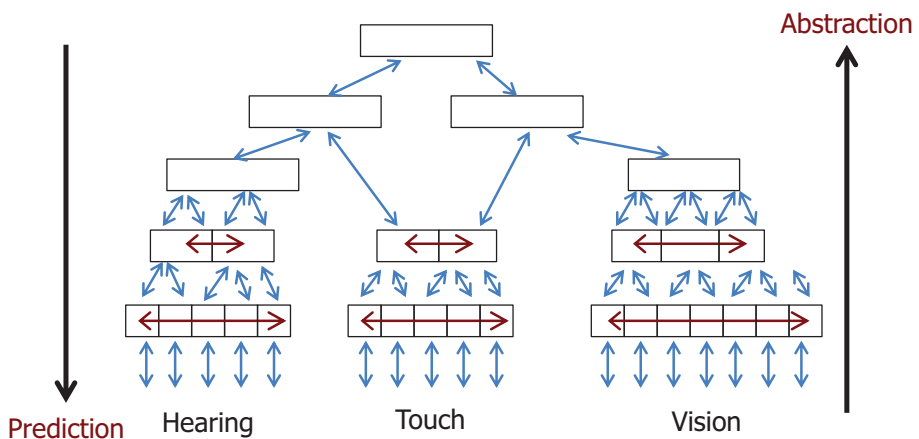


**Figure 2.4.** Hierarchical organization of the cortex. Each box in the diagram represents a set of neighboring cortical columns

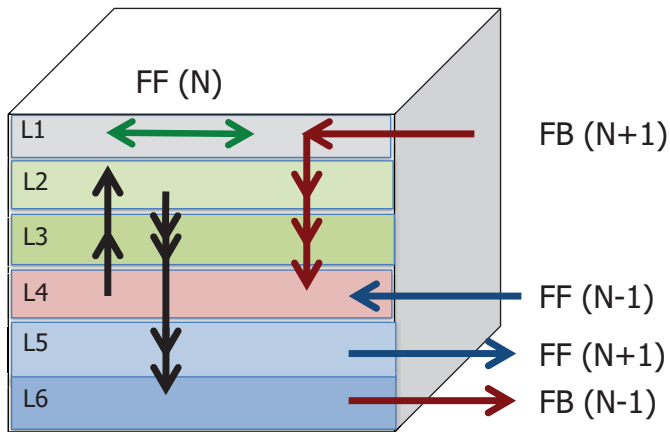


**Figure 2.5.** Internal and external connections of a cortical column. The black arrows represent the main connections between the layers of the same column. The green arrow represents the connections between columns on the same hierarchical level, the blue arrows show the direct hierarchical communications (FF: feedforward) and the red arrows show the feedback (FB)

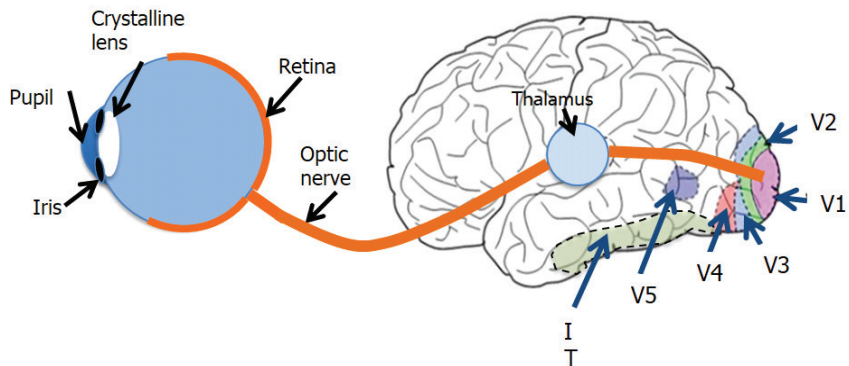


**Figure 2.6.** Organization of the human visual system. The eye diameter has been amplified

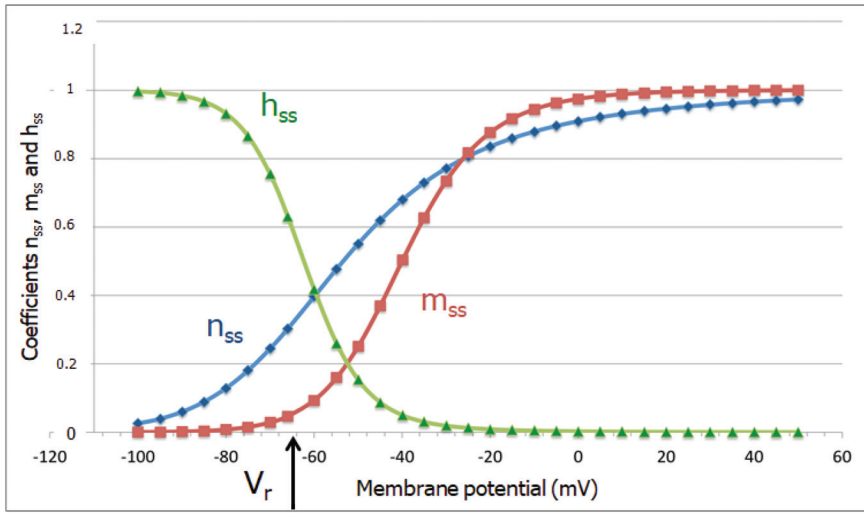


**Figure 3.14.** Coefficients  $n_{ss}$ ,  $m_{ss}$  and  $h_{ss}$ , extracted from expressions [3.24]. The arrow indicates the resting potential,  $V_r$

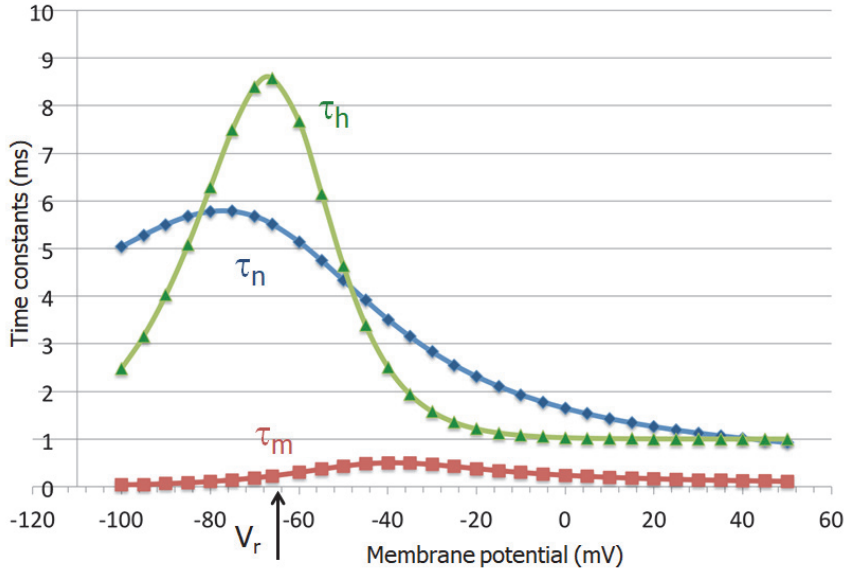


**Figure 3.15.** Time constants  $\tau_n$ ,  $\tau_m$  and  $\tau_h$ , extracted from expressions [3.24]. The arrow indicates the resting potential,  $V_r$

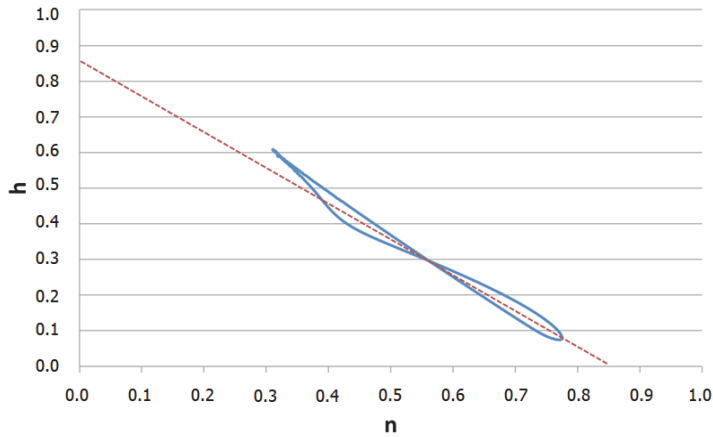


**Figure 3.21.** Coefficient  $h$  as a function of  $n$  in the event of a spike. The red dotted straight line represents the equation,  $n + h = 0.85$

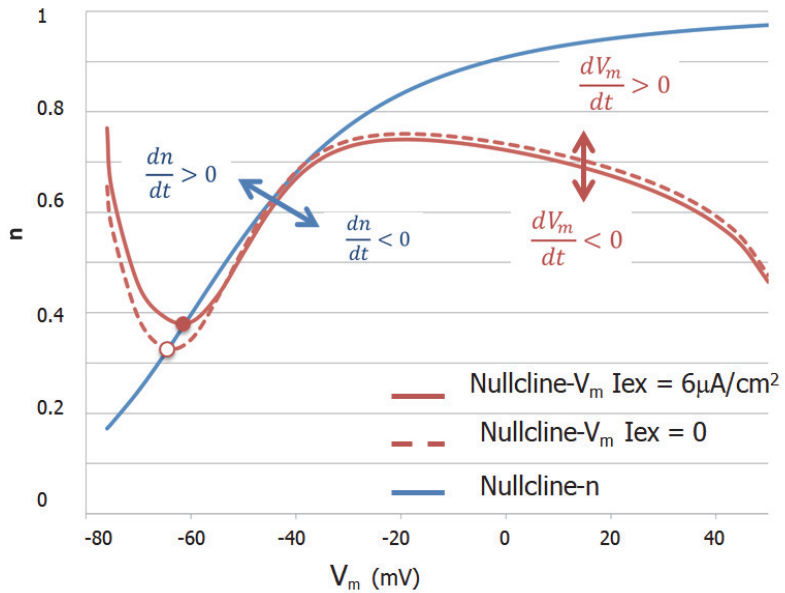


**Figure 3.22.** Nullclines of  $n$  (blue line) and of  $V_m$   $I_{ex}=0$  (red dotted line) and  $I_{ex} = 6 \mu A/cm^2$  (red solid line)

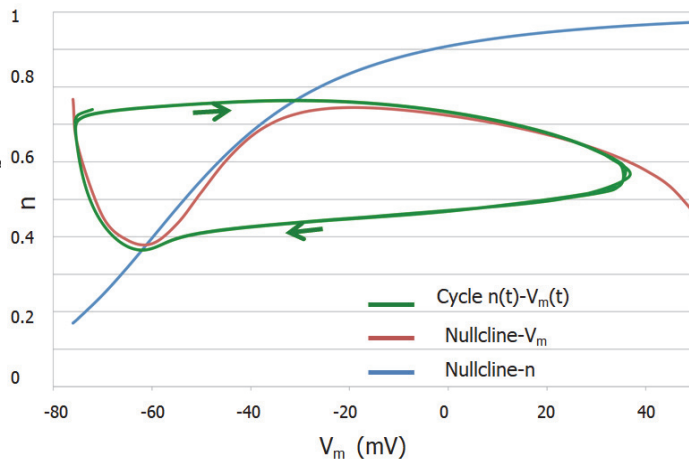


**Figure 3.23.** Nullclines of  $n$  and  $V_m$  ( $I_{ex}=6\mu A/cm^2$ ) and  $V_m(t)$ ,  $n(t)$  cycles resulting from the resolution of the Hodgkin and Huxley equations without approximation

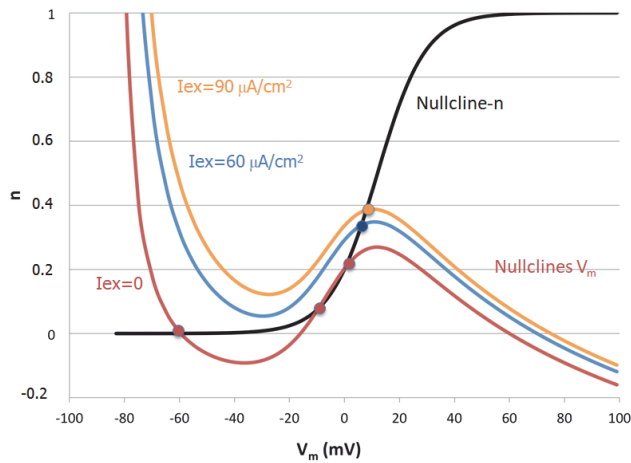


**Figure 3.24.** Isoclines  $n$  and  $V_m$  for different values of excitation current,  $I_{ex}$



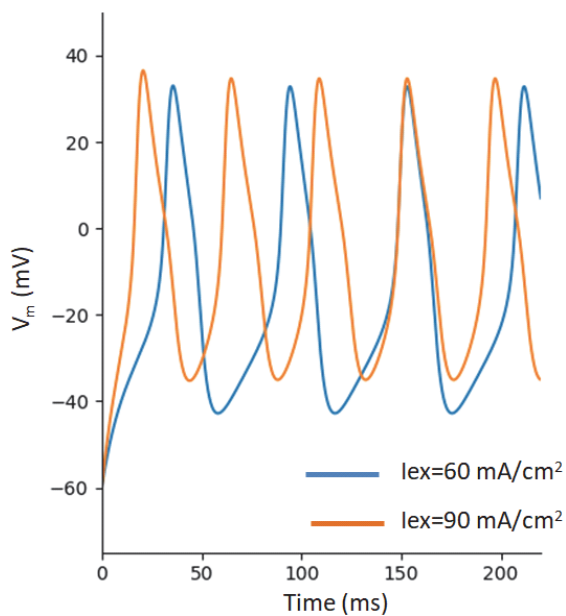


**Figure 3.25.** Action potentials of the ML model for two excitation current values

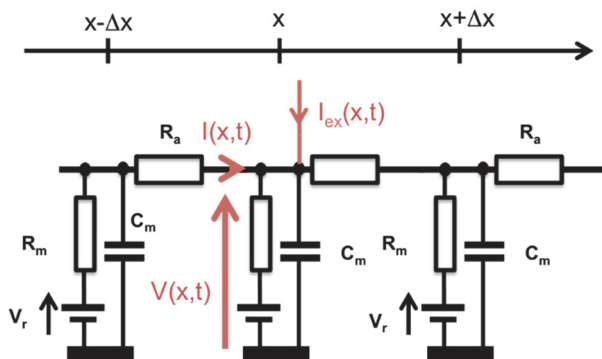


**Figure 3.27.** Axon represented by an RC line

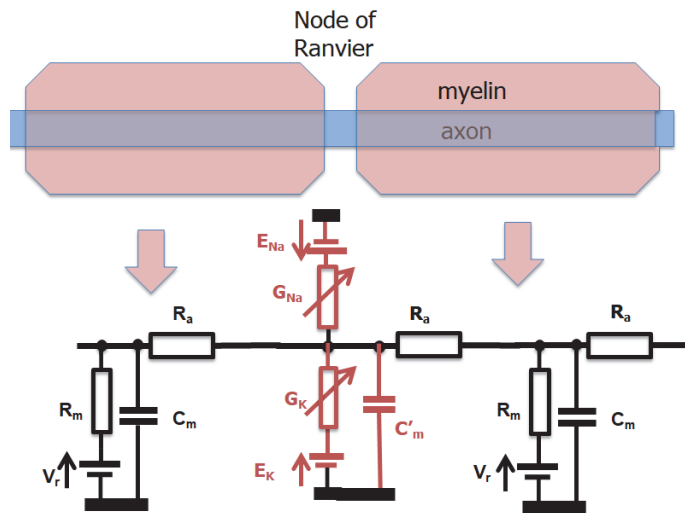


Figure 3.30. Equivalent circuit of a myelinated axon

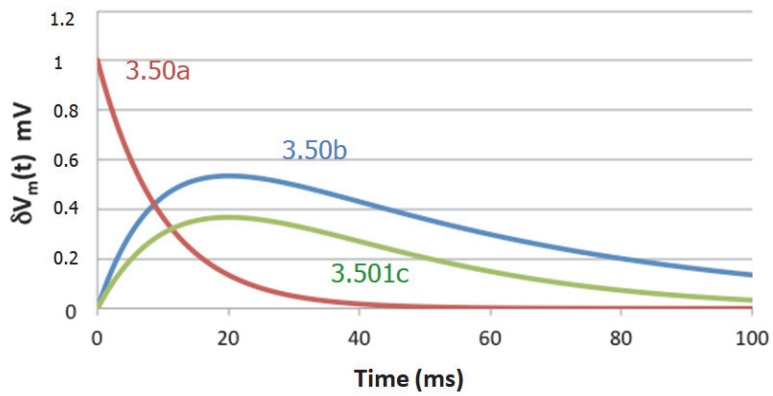
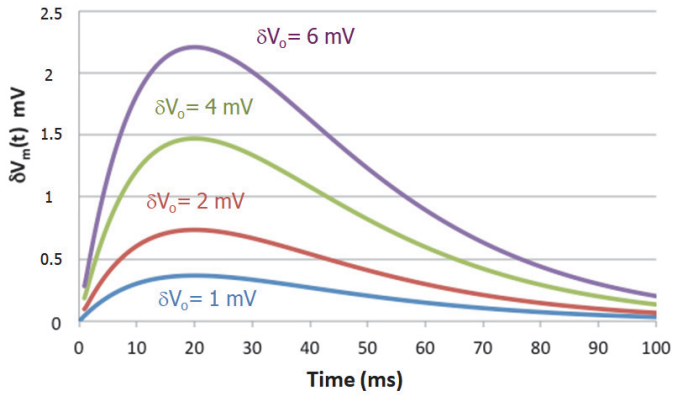
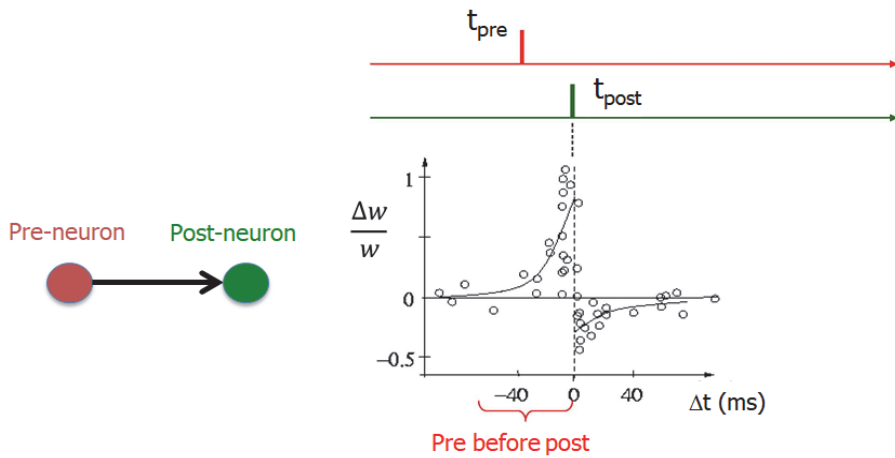


Figure 3.33. Mathematical models of EPSPs given by expressions [3.50a, b, c]



**Figure 3.34.** EPSP of an excitatory synapse for different synaptic weight values

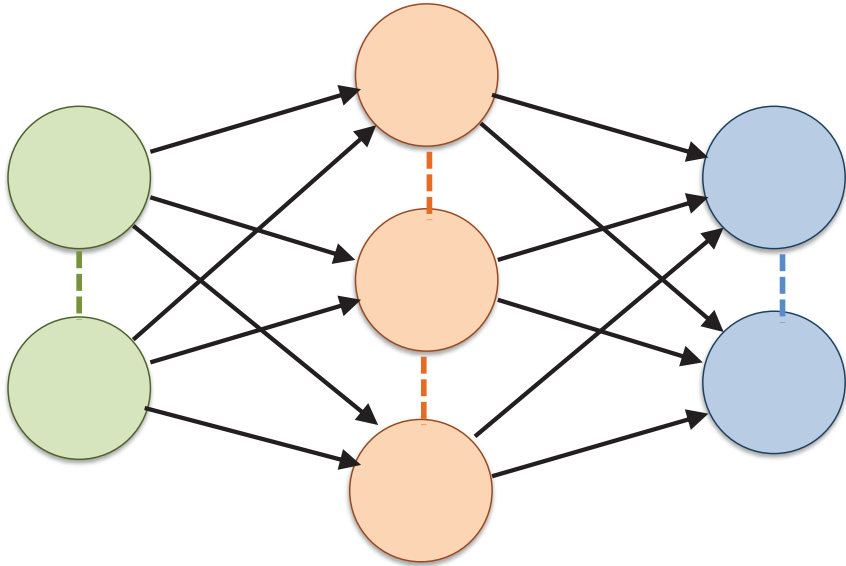


**Figure 3.35.** Principle of STDP, according to Bi and Poo.  $w$  is the synaptic weight,  $\Delta w$  represents the variation in this weight ([http://www.scholarpedia.org/article/Spike-timing\\_dependent\\_plasticity](http://www.scholarpedia.org/article/Spike-timing_dependent_plasticity))

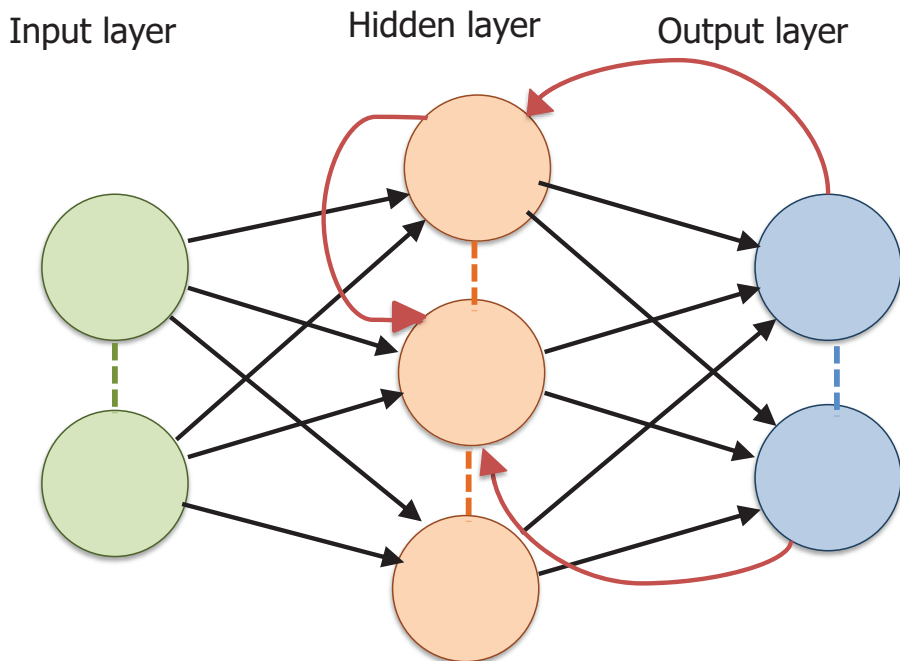
Input layer

Hidden layer

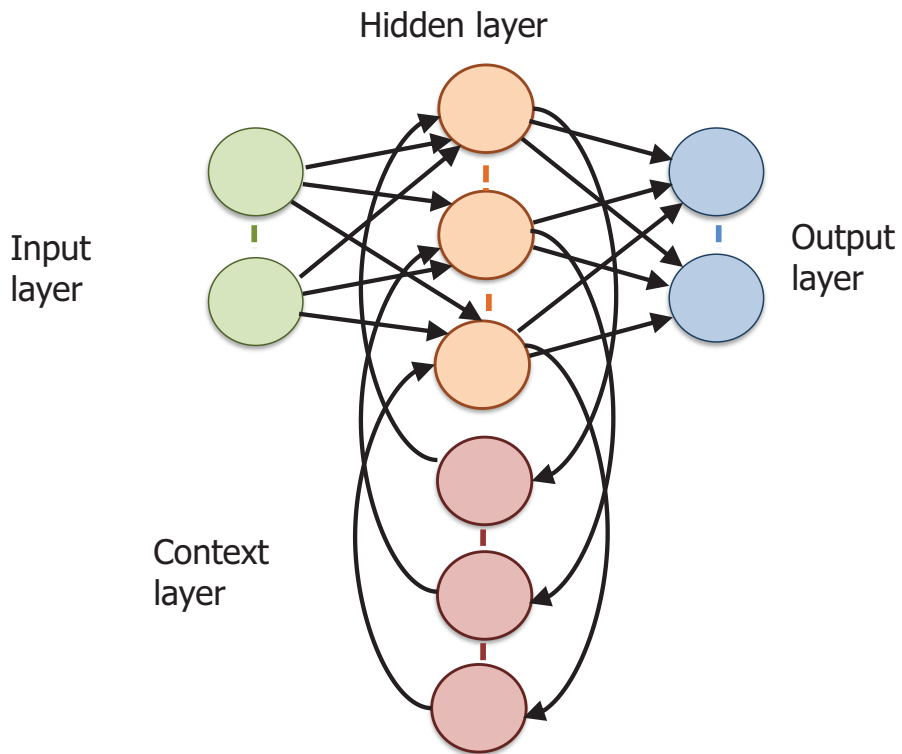
Output layer



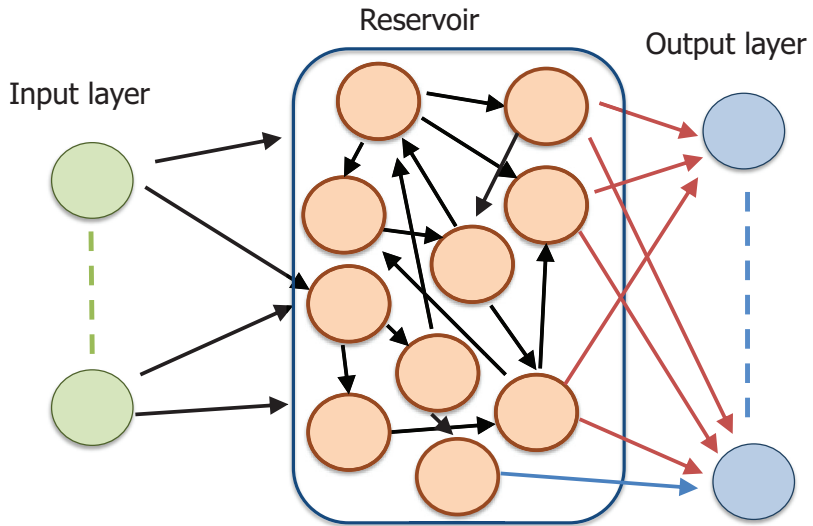
**Figure 4.2.** *Signal-flow graph of the multilayer perceptron or feedforward network with a single hidden layer. The number of neurons in each layer can be arbitrary*



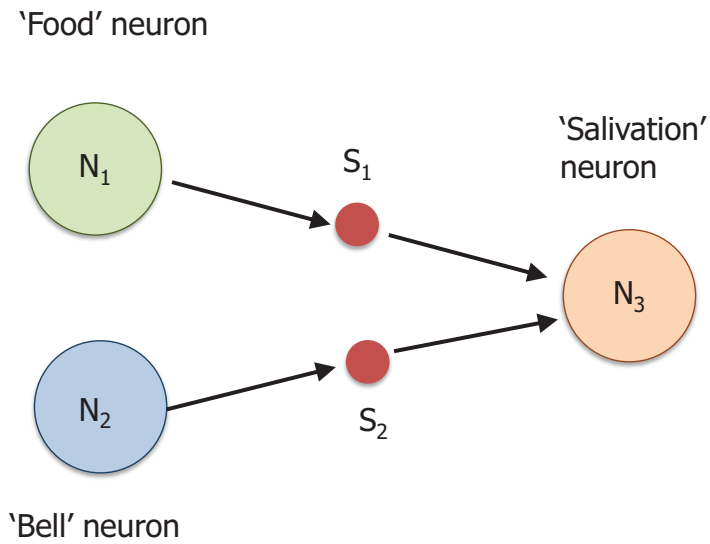
**Figure 4.4.** *Signal-flow graph of a hidden-layer recurrent neural network.  
The recurrent connections are shown in red*



**Figure 4.5.** Graph of an “Elman”-type recurrent network

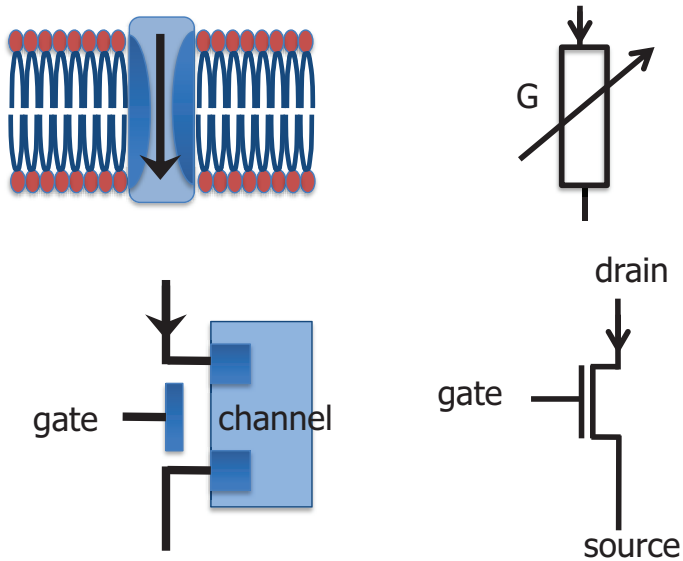


**Figure 4.7.** *Principle of reservoir computing. The black arrows represent fixed-weight synapses and the red arrows represent plastic synapses*

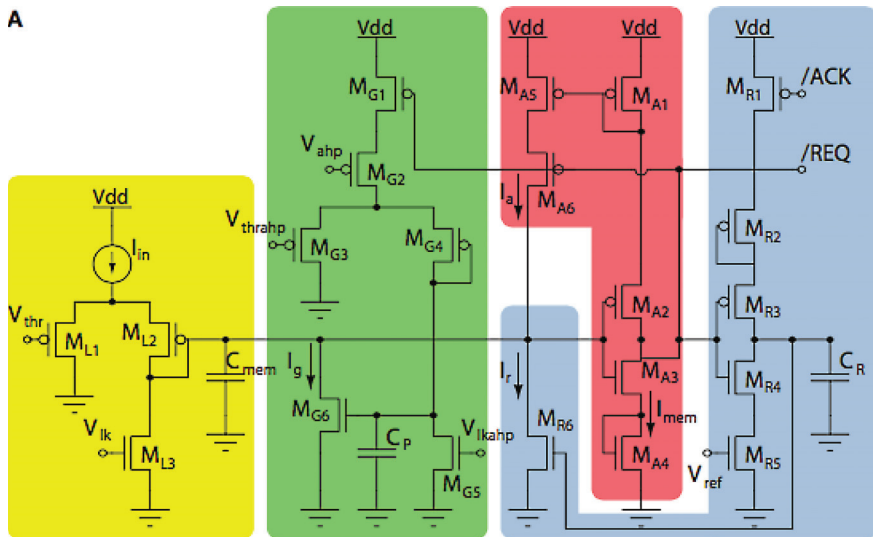


**Figure 4.8.** Modeling of the Pavlov experiment with three neurons ( $N_1$  “food”,  $N_2$  “bell” and  $N_3$  “salivation”) and two synapses ( $S_1$  and  $S_2$ )





**Figure 4.9.** *Current control by ion channel in a biological membrane and by a transistor in an electronic circuit. Physical composition and equivalent electrical circuit*

**A**

**Figure 4.12.** Diagram of a DPI neuron. The yellow block models the leakage conductance, the green block is a spike frequency adaptor, the red block simulates the sodium channels (positive feedback) and the blue represents the reset after spike generation. This figure is taken from the “Frontiers in Neuroscience” journal, May 2011, Volume 5, article 73 (Indiveri et al. 2011)

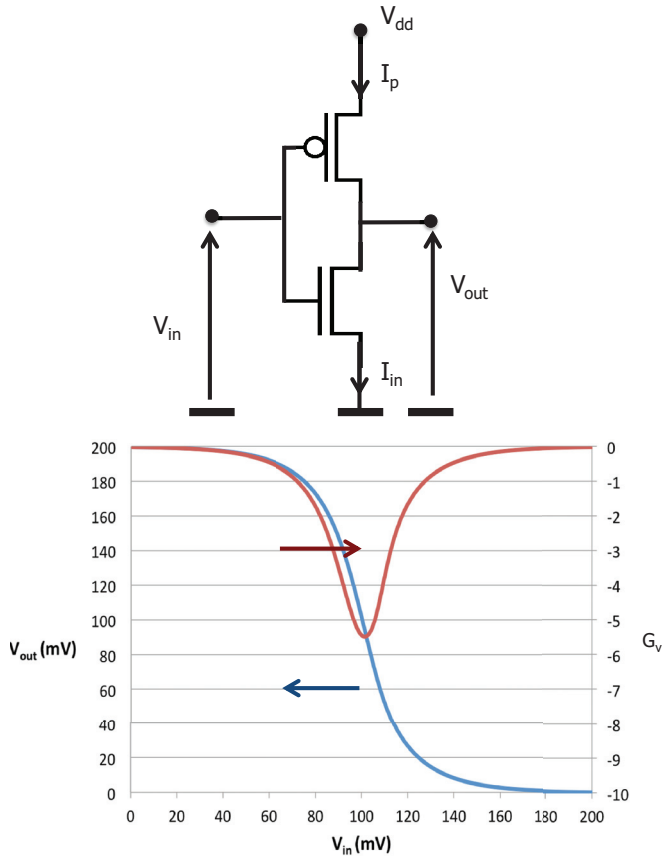


**Figure 4.13.** Circuit diagram, transfer function  $V_{out}(V_{in})$  and voltage gain  $G_v$  of a subthreshold inverter ( $V_{dd}=200$  mV). SPICE simulation for a 65 nm technological process

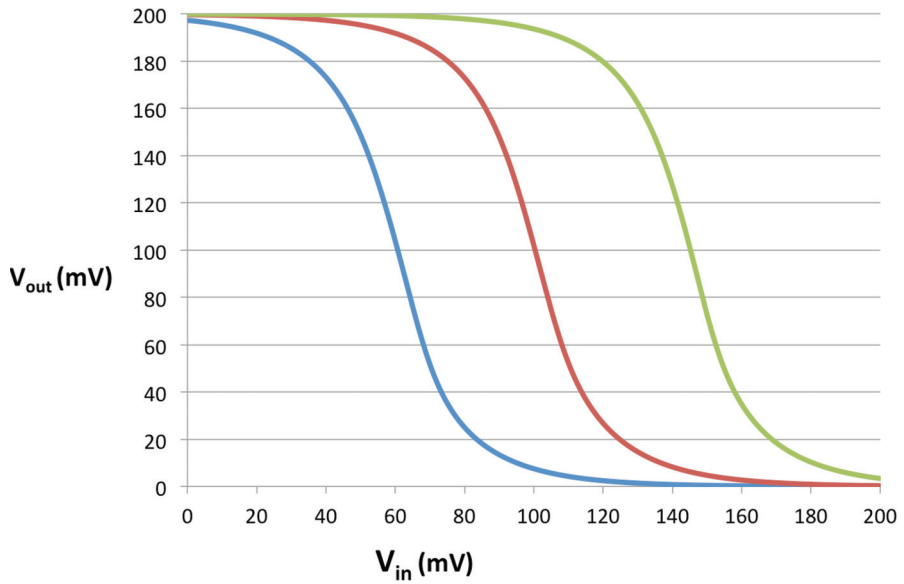


**Figure 4.14.** Transfer function,  $V_{out}(V_{in})$ , of a subthreshold inverter ( $V_{dd}=200$  mV) for different values of  $I_n/I_p$  (1 in red, 1/16 in green and 30 in blue). SPICE simulation for a 65 nm technological process

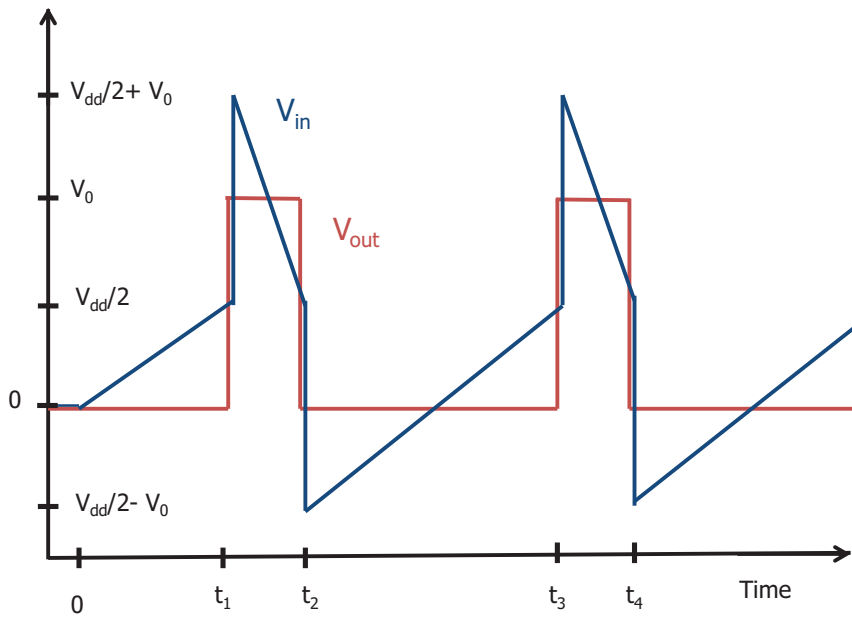


**Figure 4.18.** Time variation of potentials  $V_{in}$  and  $V_{out}$  in the case of the simplified axon-hillock model

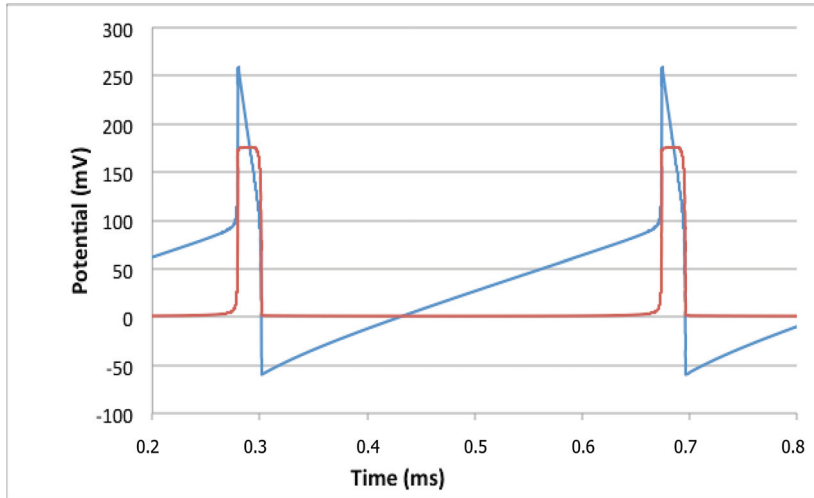


**Figure 4.19.** Time variation of potentials  $V_{in}$  and  $V_{out}$ , obtained by SPICE simulation of the circuit in Figure 5.15 for a 65 nm technological process.  $V_{dd} = 200$  mV and  $C_R = 100$  fF,  $I_{exc} = 40$  pA,  $I_R = 800$  pA

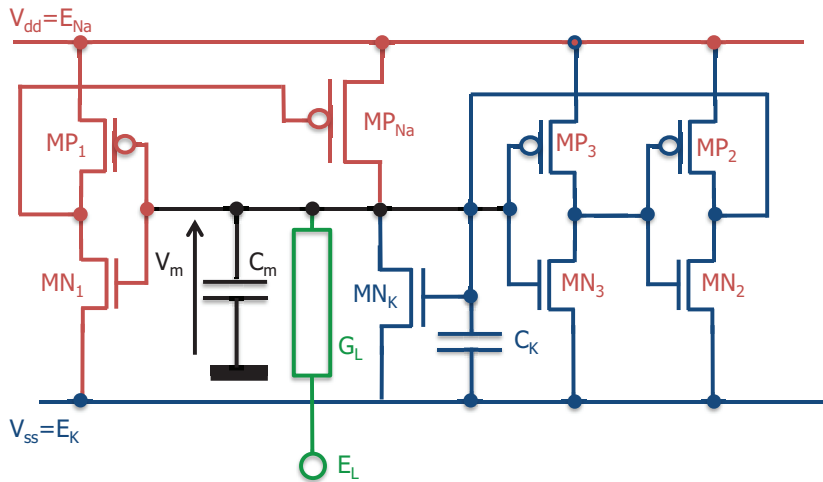


**Figure 4.21.** Complete schematic diagram of the eight-transistor electronic circuit simulating the ML model.  $V_{dd}$  represents the positive potential ( $E_{Na}$ ), and  $V_{ss}$  the negative potential ( $E_K$ ). The positive-reaction circuit (pull up) is shown in red, the feedback (pull down) in blue and the leakage conductance in green

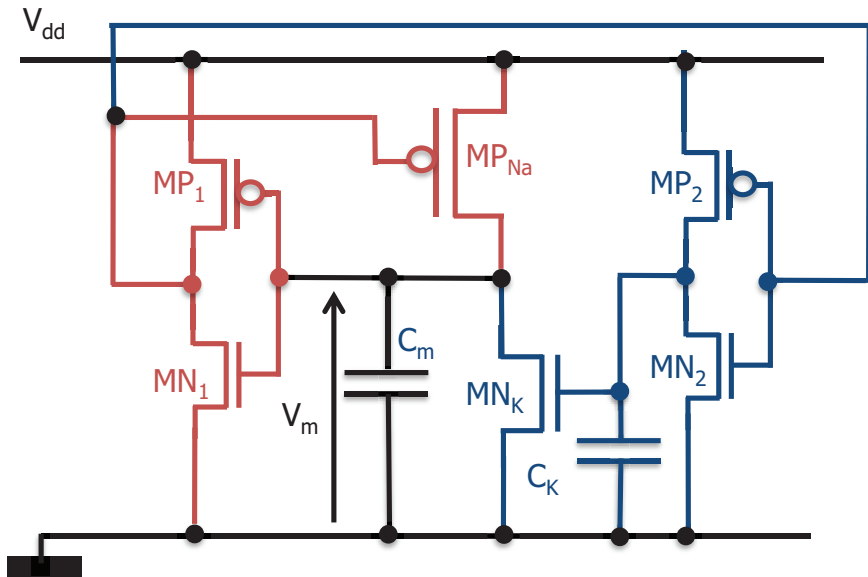


**Figure 4.22.** Simplified diagram of the ML neuron comprising only six transistors and a single power supply. The positive-reaction circuit (pull up) is shown in red and the feedback (pull down) in blue



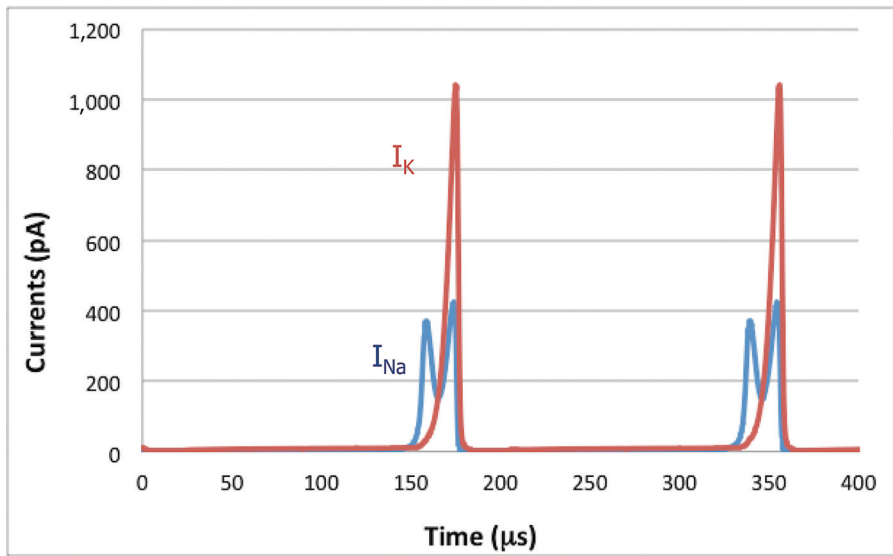
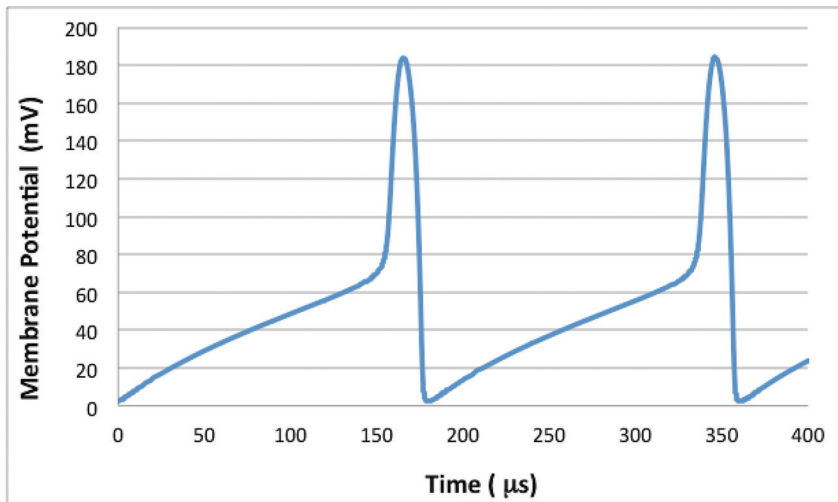


**Figure 4.23.** Temporal variation in membrane potential and sodium and potassium currents. The excitation current,  $I_{ex}$ , is constant and equal to 15 pA. These figures are taken from a SPICE simulation for a 130 nm CMOS industrial technology

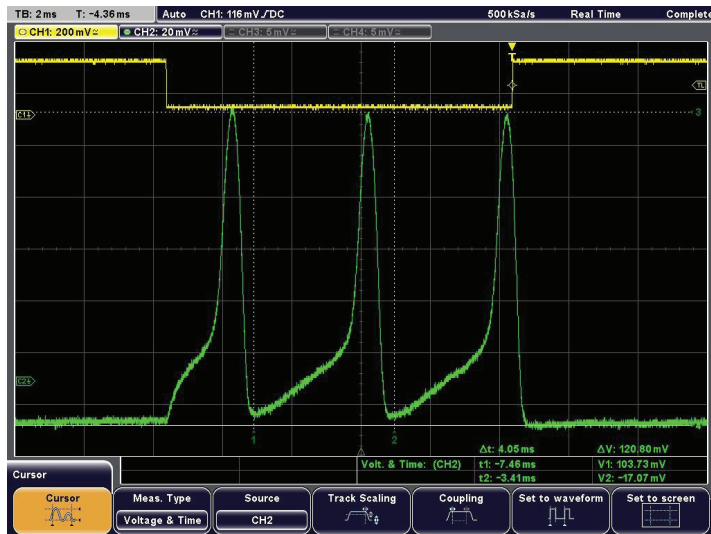
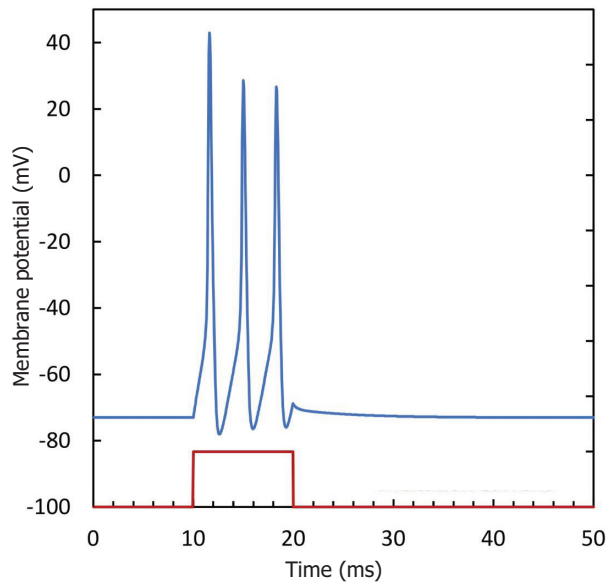


**Figure 4.24.** Comparison between a very complete biomimetic neuron model (top) and the measurement performed on the circuit (bottom). In both cases, the excitation is applied for a period of 10 ms

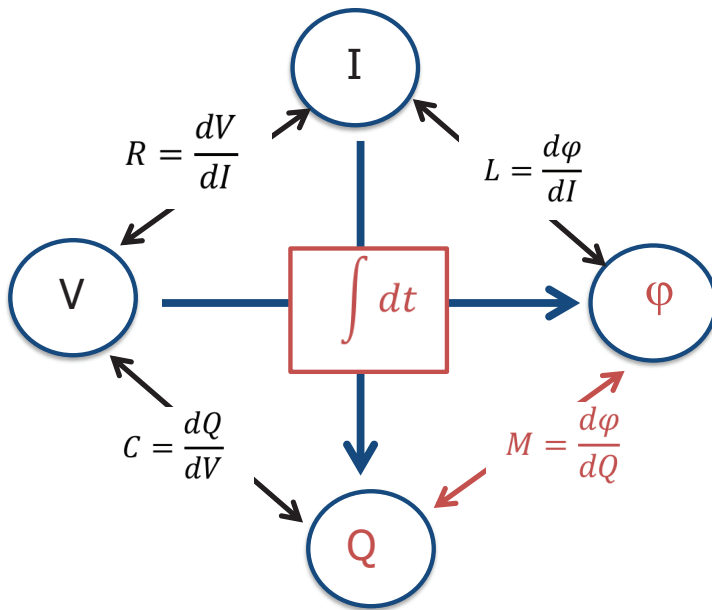


**Figure 4.26.** Definition of the memristance or fourth element based on state variables  $I$ ,  $V$ ,  $Q$  and  $\phi$  and conventional dipoles  $R$ ,  $L$  and  $C$

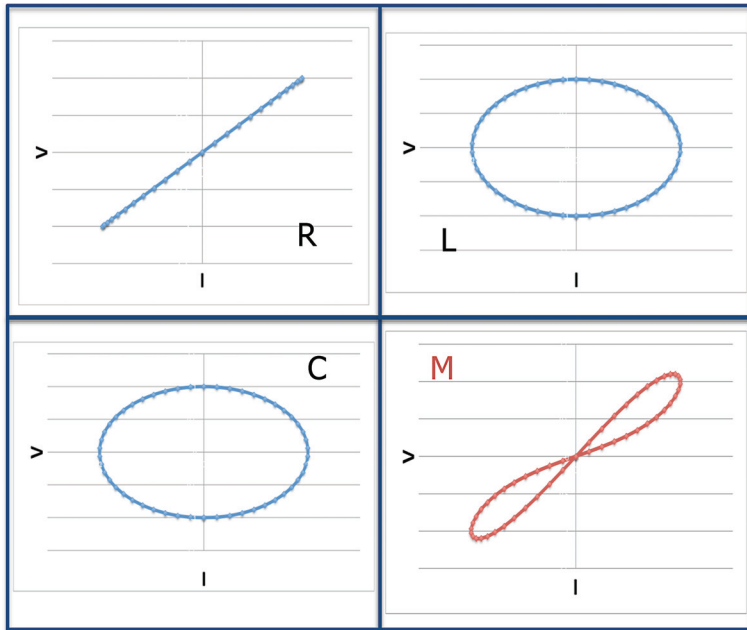


**Figure 4.27.**  $V(t)$ – $I(t)$  curves when  $I = I_0 \sin(\omega t)$ , for a resistance,  $R$ , an inductance,  $L$ , a capacitance,  $C$ , and a memristance  $M$ . For  $L$  and  $C$ , the directions of rotation are reversed (phase shift of  $\pm \frac{\pi}{2}$ ). For the memristance, we always have  $V = 0$  when  $I = 0$

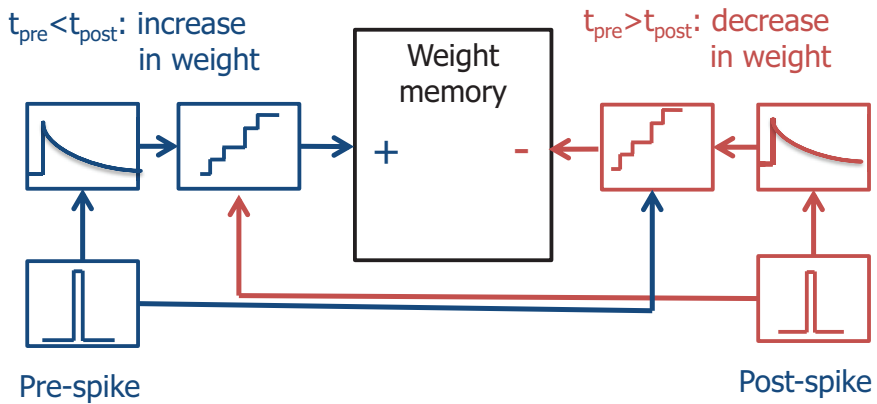


**Figure 4.28.** Architecture for the electronic implementation of the STDP.  
 The two circuits, " $t_{pre} < t_{post}$ " and " $t_{pre} > t_{post}$ ", are identical

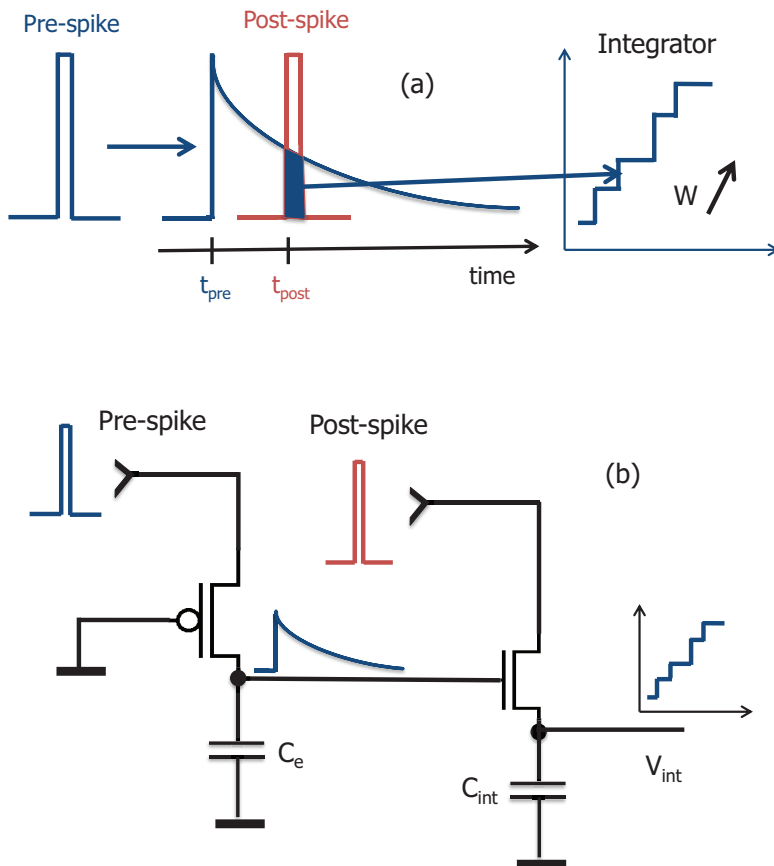


**Figure 4.29.** Principle of implementation of the STDP. (a) Scenario where  $t_{pre} < t_{post}$ , the synaptic weight increases. The pre-spike is extended, and the value of the extended spike at the instant when the post-spike is sampled and then integrated. (b) Exemplary embodiment of the extension of the spike, the sampler and the integrator in MOS technology

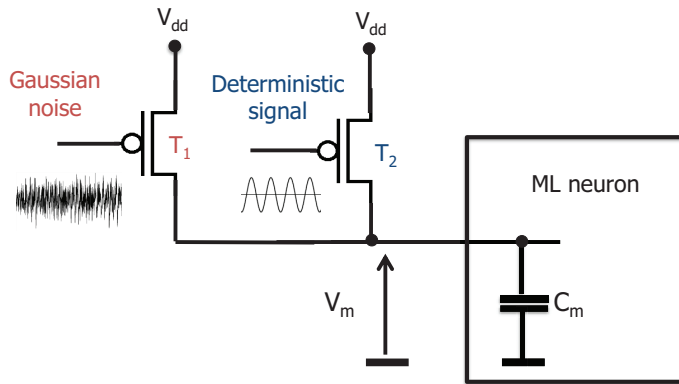


**Figure 4.30.** Circuit enabling highlighting of the stochastic resonance. Transconductance  $T_1$  represents a large number of synapses generating uncorrelated Poisson spike trains, and  $T_2$  a small number of synapses all generating the same deterministic signal

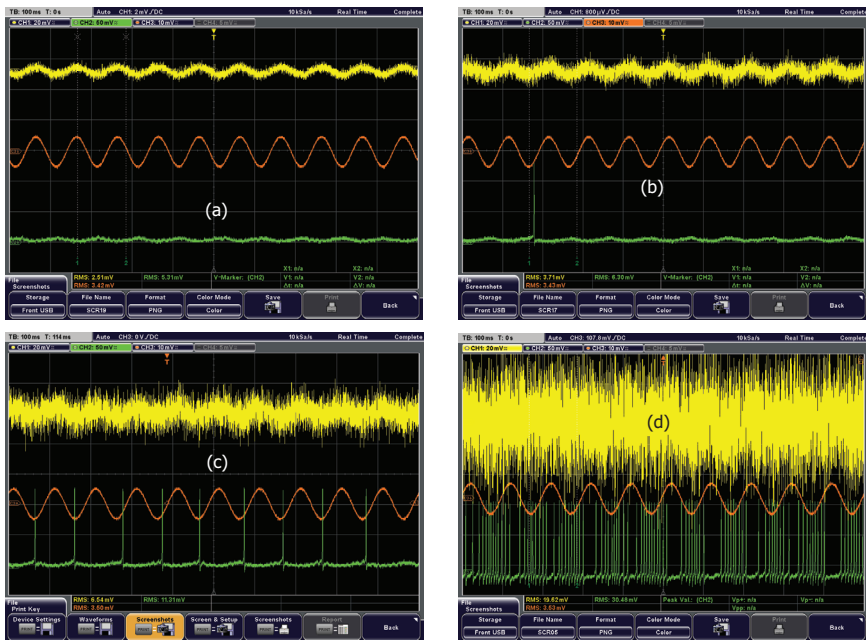


**Figure 4.31.** Response of the neuron as a function of noise power. The membrane potential is shown in green, the deterministic signal, which is constant throughout the experiment, in orange, and the “signal + noise” sum in yellow

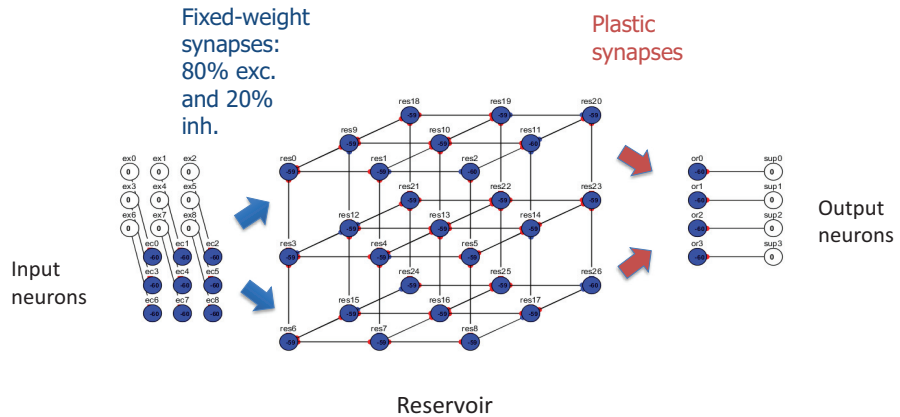


**Figure 4.32.** Simulation of a cortical column by a reservoir-computing architecture. The synaptic connections of the input layer towards the reservoir and within the reservoir are random and of fixed weight. The output neurons are connected to each of the neurons of the reservoir by a plastic synapse



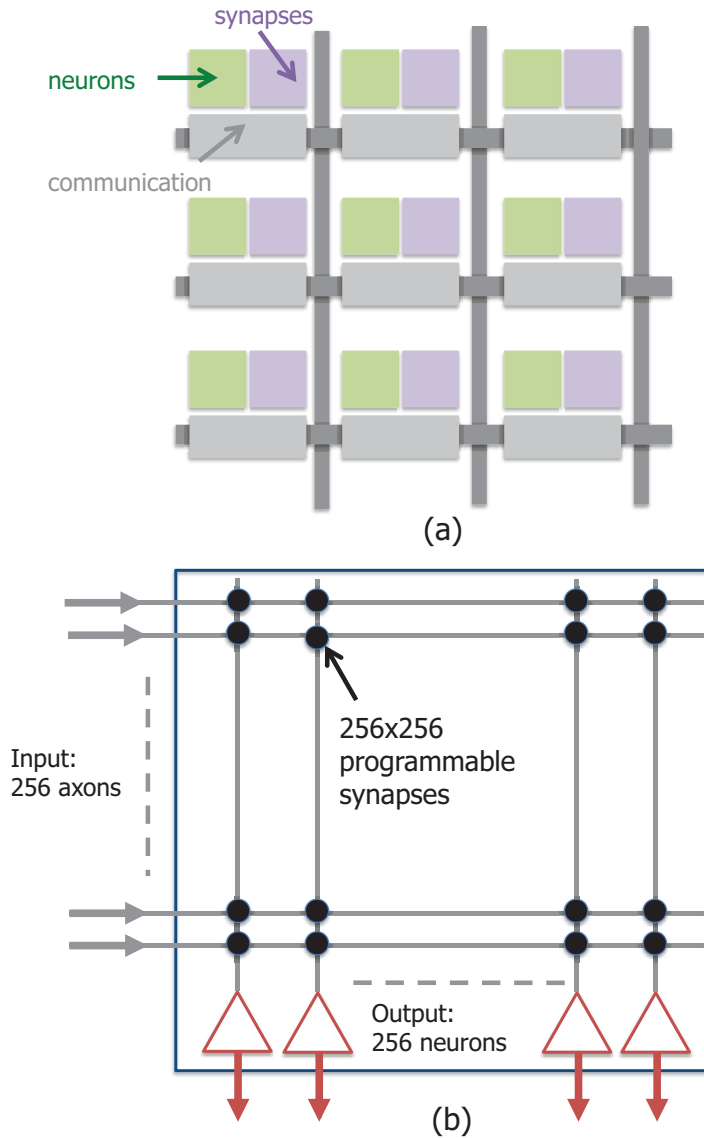


**Figure 4.33.** General architecture of the TrueNorth chip (a) and detailed architecture of a neuromorphic core; (b) (according to Merolla et al. 2014)